Fuel 387 (2025) 134385

Contents lists available at ScienceDirect

Fuel

journal homepage: www.elsevier.com/locate/fuel

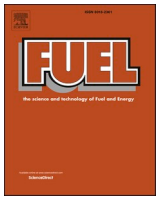

Full Length Article

Burning ammonia with methane blending in an air-staged porous media burner

Liang Li [a], Ruifang Zhang [a], Yang Zhang [a,b], Hai Zhang [a,*]

[a] Key Laboratory for Thermal Science and Power Engineering of Ministry of Education, Department of Energy and Power Engineering, Tsinghua University, Beijing 100084, China
[b] Shanxi Research Institute for Clean Energy Tsinghua University, Taiyuan, Shanxi Province 030032, China

ARTICLE INFO

Keywords:
Porous media
Ammonia combustion
Air-staging
NOx emission
Flame stability

ABSTRACT

An experimental and numerical study was conducted on the ammonia (NH_3) combustion with CH_4 blending in an air-staged porous media (PM) burner, to overcome the difficulties of low flame speed, narrow flammability and high NOx emissions in the pure NH_3 combustion. The experimental results showed that with proper settings, the proposed combustion method could achieve high power density and low emissions of NOx, unburnt NH_3 and CO. PM enhanced the flame stability, expanding flammability limit and reducing unburnt NH_3. However, the PM effect on NOx emission depended on the local equivalence ratio of the mixtures. On the fuel-lean and slight fuel-rich side, PM enhanced the NOx emission while on the highly fuel-rich side, it reduced the NOx emission. The results indicated that the air-staging to keep the primary stage in fuel-rich condition is effective for NOx emission control. Similar effect was found for the CH_4 blending but with different mechanism. The numerical simulation using a two-phase combustion model with consideration of the tortuosity well predicted the experimental results of flame stability and pollutant emissions in the PM combustion. In addition, it revealed the effect of the solid heat feedback on flame stability and NO formation. With the optimized PM structure and air-staging setting, a wide flame stable zone with low NOx, CO and NH_3 emission was realized for NH_3/CH_4 combustion.

1. Introduction

With increasing concerns of the global climate change, the carbon-free ammonia (NH_3) attracts more and more attention. Compared to hydrogen (H_2), NH_3 has a higher volumetric energy density and lower storage and transportation cost [1]. Nowadays, as a potential alternative to fossil fuels, NH_3 has been proposed to be used in various devices, including fuel cells [2], engines [3,4], coal firing furnace [5], and gas turbines [6–9]. Since combustion generally has a higher energy conversion efficiency than the cracking [10], it is a dominate way for NH_3 fuel utilization. However, the directly burning of pure NH_3 in a conventional way would encounter a few difficulties including low burning rate, narrow flammability region and weak stability, compared with the directly burning of the natural gas [11–14]. Besides, as a nitrogen-containing fuel, NH_3 combustion could produce a large amount of fuel-NOx, much higher than the hydrocarbon fuel combustion [15–17].

To increase the burning intensity, researchers suggested NH_3 could be burnt by blending with some highly reactive fuels, such as methane (CH_4) [12] or hydrogen (H_2) [13,14]. Besides reactive-fuel blending, the other way is to change combustion method. Consequently, porous media (PM) combustion, a method widely used to burn low-caloric gaseous fuels is considered. In the PM, reaction occurs in the interconnected cells of a porous-structured material. In addition to the possible surface-catalytic effect [18], the porous structure exhibits strong thermal conduction and radiation effects. Part of the heat generated by the chemical reaction is fed back to the incoming unburnt gas [19–22]. Thus, PM is in favor of realizing stable combustion in a wide flammable zone, and low CO and NOx emissions [23]. Habib et al. [24] found that when CH_4 and biogas were burnt in a PM burner, stable combustion could be realized at a low equivalence ratio $\phi = 0.275$. Sharma et al. [25] found that PM combustion could achieve a high thermal intensity of up to 3000 kW/m^2.

Recently, PM indeed was applied to burn NH_3 in laboratory. Nozari et al. [26] and Chen et al. [27] experimentally studied the NH_3/H_2 combustion in a small furnace with silicon carbide (SiC) PM blocks, in the range $0.9 < \phi < 1.5$. They found that PM was in favor of stabilizing the flame, while NOx emission was rather high (~5000 ppm) at $\phi = 1.1$ but could be sharply reduced to 35 ppm at $\phi = 1.5$. The unburnt NH_3 in the fuel-rich combustion was not reported. Vignat et al. [28,29]

* Corresponding author.
E-mail address: haizhang@tsinghua.edu.cn (H. Zhang).

https://doi.org/10.1016/j.fuel.2025.134385
Received 28 May 2024; Received in revised form 9 January 2025; Accepted 9 January 2025
Available online 14 January 2025

Nomenclature

A	Flux area (m^2)
A_f	Flame fold area factor
a_v	Specific surface area (mm^{-1})
c_p	Constant pressure specific heat capacity (J/(kg·K))
D	Porous block diameter (mm)
d_m	Mean pore diameter (mm)
h	Gas enthalpy (J/kg)
h_v	Volumetric convection heat transfer coefficient (W/(m^3·K))
$\dot{M}$	Mass flow rate (kg/s)
MW	Molar mass (kg/kmol)
Nu	Nusselt number
Q_B	Burning power density (MW/m^2)
q	Heat flux (W)
Re_d	Reynolds number
S	Flame speed (cm/s)
T	Temperature (K)
V	Volumetric flow rate (SLM)
v	Gas diffusion rate (m/s)
x	Axial coordinates (mm)
x_s	Air-stage distance (mm)
Y	Mass fraction

Greek letters

α_{NH3}	NH_3 blending ratio (in volume)
α_s	Solid material emissivity
ε	Porosity
λ	Thermal conductivity (W/(m·K))
ρ	Density (kg/m^3)
σ_e	Extinction coefficient (mm^{-1})
τ	Tortuosity
$\dot{\omega}$	Molar rate of chemical reaction production ($kmol/m^3$·s)
ϕ	Equivalence ratio

Subscripts

c	Convection
er	External radiation
g	Gas phase
ir	Internal radiation
int	Intrinsic
k	Specific gas component k
K	Total gas components
L	Laminar
opt	Optimal
P	Primary stage
PM	Porous media
s	Solid phase
T	Total
wall	Wall boundary conditions

investigated the NH_3/H_2 combustion under both fuel-lean and fuel-rich conditions ($0.5 < \phi < 1.5$) using a double-layer ceramic PM burner. High thermal power density of 62 MWm^{-3} at high NH_3 volume ratio of 70 % was realized. Low NOx emissions (<100 ppm at 15 % O_2) was achieved when combustion occurred near to the lean or rich limits, but with high unburnt NH_3 (>1000 ppm). Existing studies indicated that PM burner and H_2 blending can achieve low NOx emissions and high combustion efficiency (low unburnt NH_3) under specific conditions.

However, the availability of H_2 is limited, thus it is interest to find if CH_4, a more easily obtainable fuel could be used as a substitute. In addition, since NOx emissions can be effectively controlled under fuel-rich conditions, the air-staging, an economic way to establish the first stage combustion in fuel-rich atmosphere should be considered for NH_3 combustion in a PM burner. Though air-staging was proved to be effective and cost-effective to reduce NOx emission in NH_3-firing gas turbine simulation [30–33] and NH_3-coal co-firing jet flames [34], it was seldom to be assess in PM combustion. Thus, NH_3 was proposed to be burnt with CH_4 blending in an air-staged PM burner.

To assess the feasibility and performance of the proposed combustion method, an experimental study was conducted. The flame stability, as well as CO, NOx and NH_3 emissions at various fuel blending ratios and air-staging ratios were assessed. In the meantime, a two-phase combustion model using the parameter tortuosity to describe the PM morphology was employed to further reveal physio-chemical insights of NH_3 combustion in the PM burner. Based on the experimental and numerical results, an optimal design of the air-staged PM burner was proposed.

2. Methodologies

2.1. Experimental

An experimental system with an air-staged PM burner was set up for NH_3/CH_4 combustion. As schematically shown in Fig. 1, the system consisted of a combustion chamber unit, a gas supply unit, an image recording unit, and a measurement unit.

The combustion chamber, with dimension of 300 mm long, and ϕ52 mm in diameter was made of quartz tube for visual observation. In its bottom, two layers of sintered metal plate and a honeycomb ceramic plate were installed to keep the incoming premixed flow uniform and prevent unwanted flashback. The chamber was surrounded by an electrically heating furnace with a movable bracket to reduce heat loss and provide a controllable boundary condition.

Above the sintered metal plate, porous media (PM) blocks with diameter of ϕ50 mm and thickness of 15 mm were placed. The PMs were made of the inert silicon carbide (SiC) with porosity ε of 80 %–85 % and pore density of 10 pores per inch (PPI). The PM blocks had good thermal shock resistance, and no material failure (by XRD) found after ~ 300 h experimental operation. The pore structure of the PM was detected by industrial computed tomography (NanoVolex 4000 from Sanying Precision Instruments Co., China) with a resolution of 50 μm. Besides ε and pore size d_m, the tortuosity τ, a parameter reflecting the obstruction of the porous structure to the diffusion process was also adopted to describe the PM structure. The value of τ was obtained using the method proposed by Cooper et al. [35], and the d_m distribution was obtained using the code developed by Rabbani et al. [36]. The structural parameters of the tested PM are listed in Table 1.

NH_3 and CH_4 were mixed at a given volumetric ratio α_{NH_3}, as calculated by Eq. (1))α_{NH_3}, in the mixing chamber. Experiments were conducted at atmospheric pressure and the inlet temperature of the reactants was controlled below 50 °C.

$$\alpha_{NH_3} = \frac{V_{NH_3}}{V_{NH_3} + V_{CH_4}} \quad (1)$$

When the air-staging was applied, the air stream was fed into the PM burner in two stages, and the combustion in the PM burner was consequently divided into a primary stage and a secondary stage. In the primary stage, the mixture at a preset equivalence ratio ϕ_P entered from the bottom. The staging air was injected into the gap between two stages through a branch-type air distribution pipe. The preliminary experiments showed that the primary stage with two layers of PM blocks was conducive to achieve submerged flame and shorten burner's start-stop

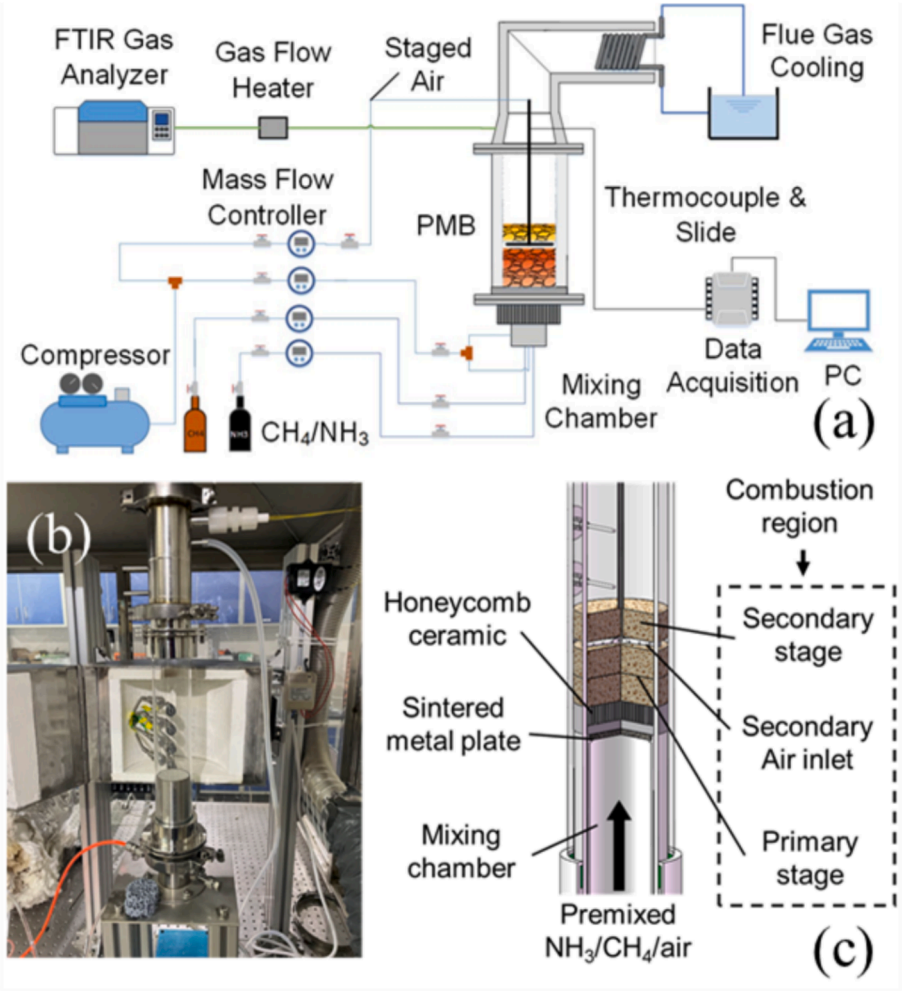

Fig. 1. The experimental system of PM combustion (a: schematic of the system; b: picture of the combustion chamber; c: schematic of the PM burner).

Table 1
The structural parameters of the tested SiC PM.

Parameter	Symbol	Unit	Value
Apparent pore density	/	PPI	10
Porosity	ε	/	0.817
Mean pore diameter	d_m	mm	3.207
Specific surface area	a_v	m^{-1}	1007
Solid tortuosity	τ_s	/	2.12
Gas tortuosity	τ_g	/	1.19

response time, while the secondary stage with a single layer PM block could enhance the flame stability. The main experiments were carried out with three layers of foam ceramic blocks, and only for those to assess the effect of the residence time in the primary stage, additional blocks of PM were added to the primary stage.

Before data acquisition, the premixed flame was stabilized in the PM burner at a preset flow condition for 30 min to ensure that the combustion reached a steady state. Then, the temperature and flue gas composition were measured three runs in 10 min, 1 min for each run. The measurement interval of the flue gas composition was 1 s, and the recorded data were processed after gross error rejection. Flue gas was sampled at the burner outlet using a flute-tube type probe and then introduced into the measurement instrument with a temperature higher than 150 °C to ensure accurate NH_3 detection. The concentrations of NO, NO_2, N_2O, CO, CO_2, and NH_3 were measured simultaneously by a Fourier Transform Infrared (FT-IR) spectrometer (Thermo Scientific Nicolet iG50 Spectrometer) with the resolution of 0.5 cm^{-1}, corresponding to an accuracy of ~ 1.0 ppm. At the same time, the temperature profiles in the PM burner were measured by a K-type thermocouple. Through visual flame observation and temperature monitoring, the stability of the flame was determined.

The uncertainties for the measurement results were estimated as three times the standard deviation (SD) plus the systematic error. The equivalence ratio obtained from the actual flow rate measured by mass flow controller (MFC). Reproducibility of the data was, on average, within 4 % of each mean value. The emission results were converted to dry base conditions at 3.5 % O_2.

The primary stage equivalence ratio ϕ_P was varied from 0.8 to 1.6 to investigate the effects of different air-staging conditions on combustion performance. The secondary air was mixed with combustion products of the primary stage, while the total equivalence ratio ϕ_T was maintained constant. The total equivalence ratio ϕ_T was maintained at 0.8 to ensure fuel-lean condition and complete fuel combustion. Additionally, the power density Q_B was kept constant at 0.5 MW/m^2 for NOx emission experiments. To investigate the effect of PM on combustion stability, experiments were conducted without PM blocks under the same inlet conditions.

2.2. Numerical approach

To reveal more detail insights of NH_3 combustion in PM, a two-phase model [37] was adopted with more detailed consideration of PM structure characteristic. In the model, the solid ceramic struts and

combustion in cavities were divided into solid and gas phases. Thermal conduction and most radiation occurred in solid phase. The chemical reactions were limited in the gaseous phase. The model was used to predict the burning rates and combustion products in the steady-state PM combustion under different boundary conditions. If the flame could be stabilized at higher flow rates, with the combustion heat feedback balanced with the preheating of the unburned gas, then combustion stability was regarded to be improved.

Providing that thermal conductivity of PM was high, one-dimensional (1-D) flame approximation was adopted for the primary stage. The 1-D approximation allows the model to more efficiently simulate the effect of heat transfer enhancement in PM on pollutant formation in NH_3 combustion.

The gas combustion process is governed by the following continuity equation.

$$\frac{d\dot{M}}{dx} = 0 \tag{2}$$

Species conservation equation is

$$\dot{M}\frac{dY_k}{dx} + \frac{d}{dx}(\rho A \varepsilon Y_k v_k) - A\varepsilon\dot{\omega}_k MW_k = 0 \tag{3}$$

Gas-phase energy conservation equation is

$$\dot{M}c_{p,g}\frac{dT_g}{dx} - \frac{d}{dx}\left(\lambda_g A\varepsilon\frac{dT_g}{dx}\right) + \sum_{k=1}^{K}\rho A\varepsilon Y_k v_k c_{p,k}\frac{dT_g}{dx} + \sum_{k=1}^{K}A\varepsilon\dot{\omega}_k h_k MW_k + \frac{d}{dx}(q_c) = 0 \tag{4}$$

Solid-phase energy conservation equation is

$$-\frac{d}{dx}\left(\lambda_s A(1-\varepsilon)\frac{dT_s}{dx}\right) - \frac{d}{dx}(q_c) - \frac{d}{dx}(q_{ir}) + \frac{d}{dx}(q_{er}) = 0 \tag{5}$$

where, ε is the PM porosity, representing the percentage of gas (void) phase.

The gas–solid two-phase heat transfer includes solid thermal conduction, gas–solid convection q_c, solid internal radiation q_{ir} and external wall radiation heat loss q_{er}. Since the flow resistance of PM burner is rather little, it is not considered.

The solid thermal conduction counted in the influence of the solid phase temperature and the morphology. The solid thermal conductivity λ_s is calculated by Eq. (6):

$$\lambda_s = \lambda_{s,int}(T)^* \frac{1}{\tau^2} \tag{6}$$

where, τ is the tortuosity of the solid porous structure, a characteristic parameter describing the flow obstruction due to PM morphology.

Gas-solid convective heat transfer is characterized by the volumetric convective heat transfer coefficient h_v. For SiC foam ceramics, because of similar morphology as in the literature, the empirical formula derived based on icosahedral structure by Wu et al. [38] is used:

$$q_c = \Delta x A h_v (T_s - T_g) \tag{7}$$

$$Nu = 2.0696\varepsilon^{0.38} Re_d^{0.438} \tag{8}$$

$$a_v = \frac{15.71 - 52.45\varepsilon + 79.51\varepsilon^2 - 41.5\varepsilon^3}{d_m} \tag{9}$$

The previous study showed formula Eqs. (8)–(9) is valid for $70 < Re < 800$ and $0.66 < \varepsilon < 0.93$ [35], so it would be suitable for the present study.

Since radiation in the solid PM is intensive, the Rosseland approximation model [39] is used to calculate the associated radiation heat transfer, as:

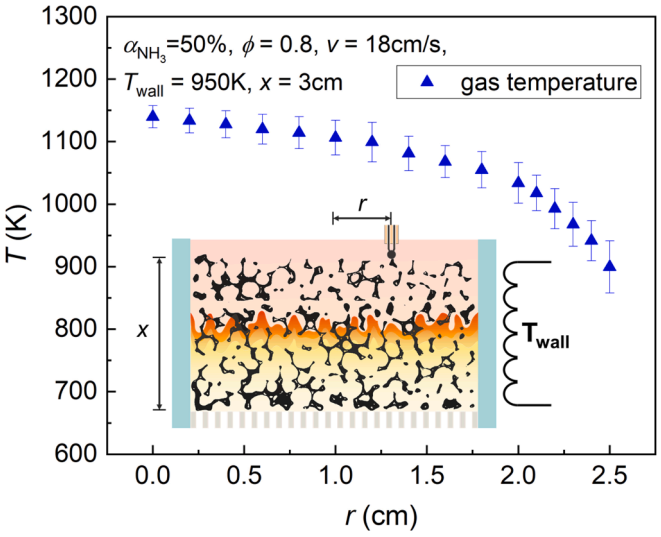

Fig. 2. Radial gas temperature distribution on the surface of PM.

$$q_{ir} = A\frac{16\sigma T_s^3}{3\sigma_e}\frac{dT_s}{dx} \tag{10}$$

$$\sigma_e = \frac{-\ln(1-\alpha_s)}{d_m}(1-\varepsilon) \tag{11}$$

where, σ_e is the extinction coefficient, obtained by using the formula given by Howell et al. [37], and α is the emissivity of the porous material.

The external radiation heat loss is calculated based on the thermostatic wall constraints, namely,

$$q_{er} = \Delta x \pi D d_m a_v \alpha_s \sigma (T_s^4 - T_{wall}^4) \tag{12}$$

where, D is the PM diameter and T_{wall} is the wall temperature. T_{wall} was the same as the experimental furnace temperature and set to 675 °C in the model. The actual emitting area in the circumferential direction of the PM was used to calculate the radiation heat loss.

In the experiments, it was difficult to measure the radial temperature distribution inside the PM during the combustion. Instead the radial temperature profile at the PM exit was measured. Fig. 2 showed temperature at the exit was rather uniform except in the area very close to wall, where some heat loss still existed. Given the flame behavior and the combustion performance were dominated by the central area with uniform temperature distribution, for simplification, 1-D approximation was reasonable for the simulation.

The developed model simulated PM combustion under different length of the primary stage zone (x_s). The calculated results were then incorporated into a chemical reactor network (CRN) model in CHEMKIN software to simulate the combustion in the secondary stage. The CRN model has two perfectly stirred reactors (PSR) and one plug flow reactor (PFR). It could separately simulate the air-staging combustion and the secondary-stage-only combustion.

Several reaction mechanisms for NH_3 combustion, including those of CEU-NH_3 [12], Okafor [40] and Konnov [41], were considered by this study. The comparisons between the predicted laminar flame speeds and the experimental data reported in the literature were used to justify the reaction mechanism selection. As shown in Fig. 3, the laminar flame speeds (calculated by CHEMKIN) predicted by CEU-NH_3 mechanism well agree with the experimental data provided by Li et al [42]. CEU-NH_3 mechanism was presented in 2021, and it used the C-N reactions given in the updated Konnov mechanism to consider the coupling of hydrocarbon and NH_3 reactions. In addition, as reported, CEU-NH_3 mechanism could well predict the combustion behaviors for NH_3

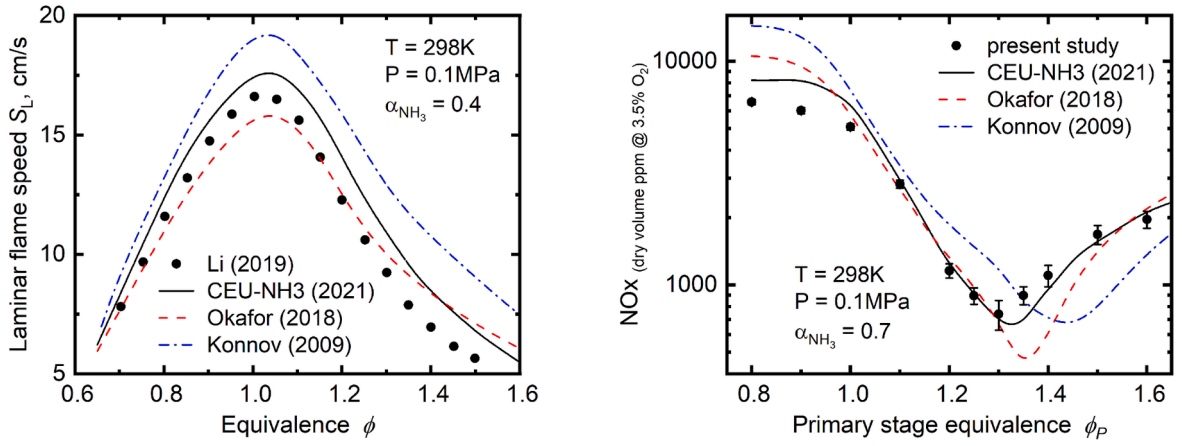

Fig. 3. Laminar flame speed and NOx emission from experiments in comparison to model predictions using different mechanisms.

Table 2
Different combustion modes for PM and open space combustion ($\alpha_{NH_3} = 70\%$).

Combustion modes	Stable flame			Unstable flame
	Submerged flame		Attached flame	Lift-off/Blow-out
Condition	$\phi_P = 0.8$ $Q_B = 1.0$	$\phi_P = 1.2$ $Q_B = 1.0$	$\phi_P = 1.6$ $Q_B = 1.0$	$\phi_P = 0.8 \sim 1.6$ $Q_B = 2.0$
Schematic	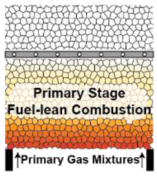	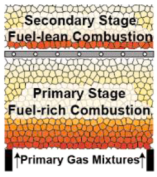	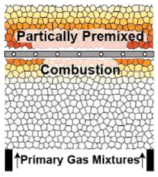	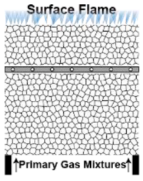
Flame images with PM				
Flame images w/o PM		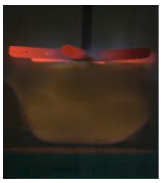		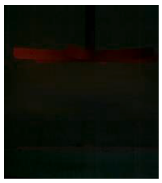

blended with CH_4 or CH_3OH. Thus, CEU-NH_3 reaction mechanism was selected for the NH_3/CH_4 combustion.

With the developed model, the temperature profile and flue gas composition in the PM burner were obtained. The maximum burning rate could be calculated by using Newton iterative approach based on temperature constraint. The model incorporates an adaptive mesh iteration method governed by grid quality parameters. A grid independence assessment was conducted and indicated a negligible variation when the grid count exceeded 300. In the simulations, the grid count for the flame was maintained between 300 and 500. The upper limit of one-dimensional laminar flame speed at the preheat temperature, so-called the preheated PM flame speed S_L^{PM} could be calculated and the flammability limit could be determined following the approach used by Zhang et al. [43].

3. Result and discussion

3.1. General flame behaviors

Table 2 shows the typical combustion mode of NH_3/CH_4 combustion at a fixed α_{NH_3} in the PM burner with air-staging. The combustion behaviors are compared with those in PM-free combustion at the same conditions. When no air-staging was used in PM combustion ($\phi_P = 0.8$), the stability of the flame could be judged by whether the flame was submerged in the PM or blown out to form a surface flame. With air-staging, because of the heat feedback from the secondary stage, flame in the primary stage could be more resilient and intended to attached on the top surface of the PM in the primary stage.

This mode of stable flame was called attached flame mode thereafter. When ϕ_P increased, the submerged flame in the primary stage moved downstream, and became an attached flame. With PM, flame could be kept in the downstream of the porous blocks, while in open space, the

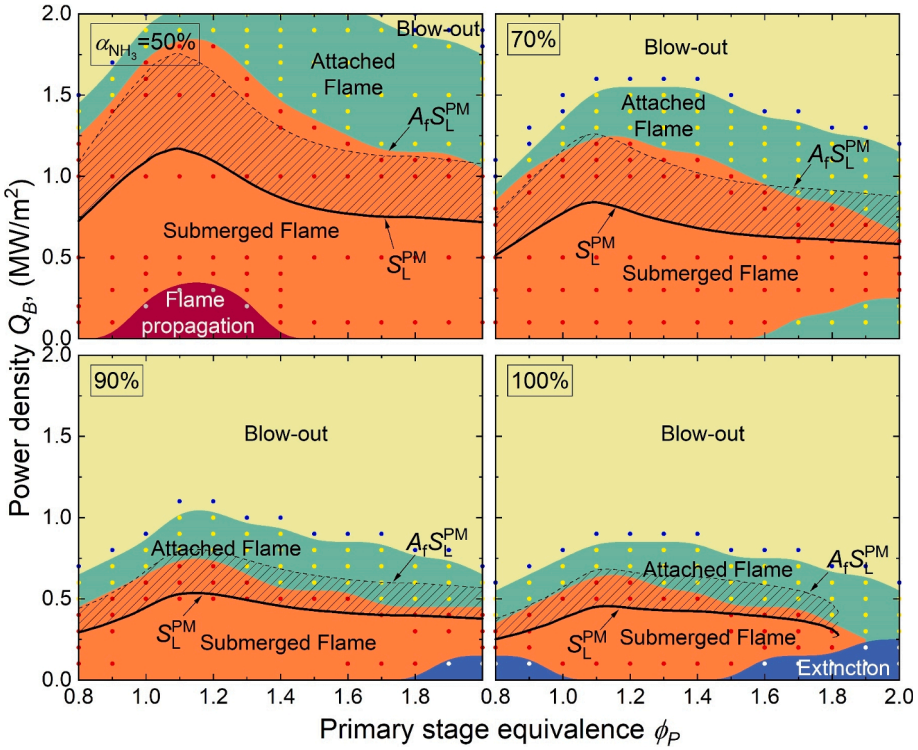

Fig. 4. Combustion stability diagram for different NH_3 blending ratio α_{NH_3} and different air-staging conditions ϕ_P in the PM burner.

flame was easily blown out of the burner. The results indicated that PM possessed a flame retention effect.

3.2. Flame stability

Fig. 4 shows the combustion stability diagrams based on the experimental measurements and model predictions. It can be seen the highest power densities appears in $1.0 < \phi_P < 1.4$. As α_{NH_3} increases, the range of stable flame becomes narrower. In the case of a low α_{NH_3} ($\alpha_{NH_3} = 50\%$), there is a risk of flashback. The flames could propagate into the honeycomb ceramics when $1.0 < \phi_P < 1.4$ and the flow rates are low. With a high Q_B, flames could stay in the secondary stage, forming attached flames rather than being blown off. With a high α_{NH_3} ($\alpha_{NH_3} > 90\%$), extinction occurs in the PM for the weakly-burning flames ($\phi_P < 1.0$ or $\phi_P > 1.4$) with low power density, as the heat generated by combustion is less than the heat dissipation of the PM block.

When honeycomb ceramics with large d_m was used, the conical flame structures in PM were observed. It was reasonable to assume that a similar phenomenon exists in foam ceramics, though difficult to be observed and measured. The solid line in Fig. 4 represents the model-derived preheated PM flame speed S_L^{PM}. The dashed line represents the predicted submerged burning rate, which was calculated by multiplying an estimated flame fold area factor A_f. In PM burner, the flame may propagate as a fully developed inclined combustion wave [44]. Based on the assumed conical flame structure and the size of the PM block, A_f was estimated to be 1.5, and the predicted submerged burning rate ($A_f S_L^{PM}$) well fit the trend of the measured ones. At a low α_{NH_3}, the predicted values are lower than the experimental results, while at high α_{NH_3} the predicted values are higher than the experimental results. The results suggest that the microscopic flame shape in PM vary with reaction rate or temperature, which should be considered in the future study.

For pure NH_3 combustion ($\alpha_{NH_3} = 100\%$), the flammability limit was calculated. The fuel-rich flammability limit for NH_3 is about 1.8, consistent with the experimental data.

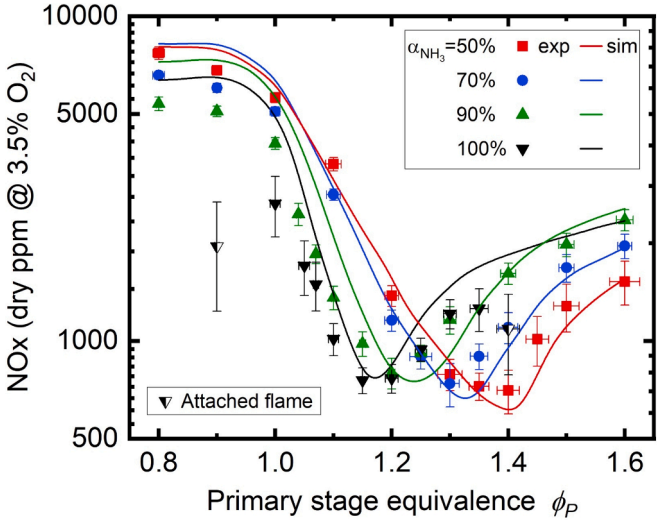

Fig. 5. NOx emissions at different α_{NH_3} in the air-staged PM burner ($Q_B = 0.5$ MW/m^2).

3.3. Pollutant emission

Fig. 5 shows the experimental and simulation results of NOx emissions for NH_3 blended fuels in the PM burner with air-staging. Total NOx is obtained by summing NO, NO_2 and N_2O. Both experimental and simulation results show that air-staging reduces NOx emissions, and there is an optimal ϕ_P, symbolized as ϕ_{opt} at which NOx emissions is minimized. This V-shaped NOx emission trend is consistent with the previous findings in PM-free NH_3 air-staged combustion [27,28]. At a fuel-lean or slightly fuel-rich condition, a large amount of NOx is formed in the primary stage under an oxidizing atmosphere, and hardly be reduced in the secondary stage. At a rather fuel-rich condition, the excessive fuel reduces flame temperature and thereby reaction rate in

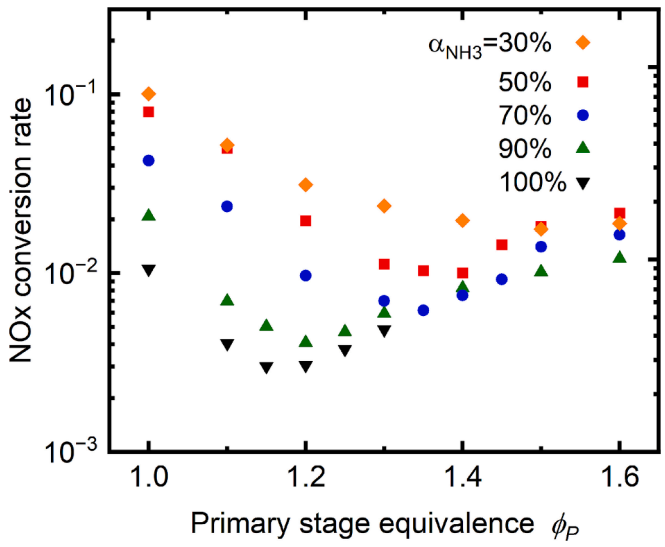

Fig. 6. NOx conversion rate at different α_{NH_3} in the air-staged PM burner (Q_B = 0.5 MW/m^2).

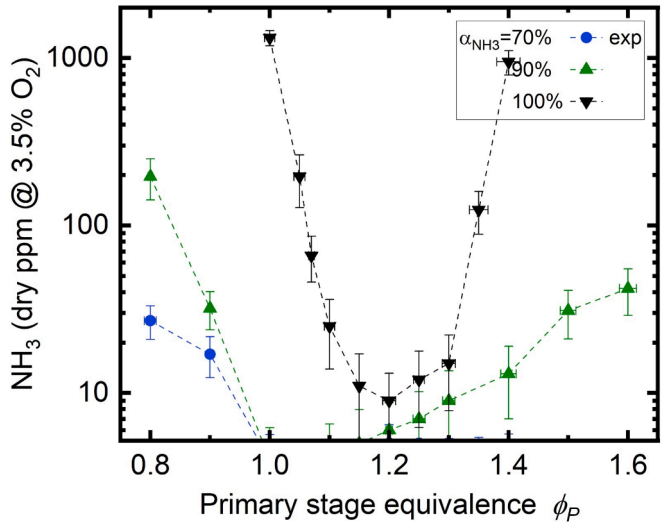

Fig. 7. Unburnt NH_3 emissions at different α_{NH_3} in the air-staged PM burner (Q_B = 0.5 MW/m^2).

the primary stage, resulting in a significant amount of unburnt NH_3. The unburnt NH_3 is then burnt in the secondary stage at a fuel-lean condition, generating a large amount of NOx over there. To minimize NOx emissions, it is essential to ensure that the primary stage combustion is intensive to keep unburnt NH_3 sufficiently low while avoiding excessive NOx generation.

As α_{NH_3} increases, the minimum values for NOx emissions becomes larger and the ϕ_{opt} decreases (moving to fuel-lean state). A higher α_{NH_3} means more CH_4 is substituted by NH_3, and thus nitrogen content in the fuel mixture increases. Even with air-staging, certain amount of nitrogen will be converted into NOx. The high nitrogen content causes a small ϕ_{opt} and a high NOx concentration at ϕ_{opt}. The phenomena can be explained by the balance between combustion intensity and oxidizer consumption. In fact, when NH_3 and CH_4 are completely burnt, they need nearly the same amount of air to keep at the same power. Since NH_3 has a lower reaction rate, when α_{NH_3} is higher, the overall reaction rate slows down, resulting in less NOx generation on the ϕ_{opt}'s left side, while the unburnt NH_3 in the primary stage increases as the fuel becomes richer.

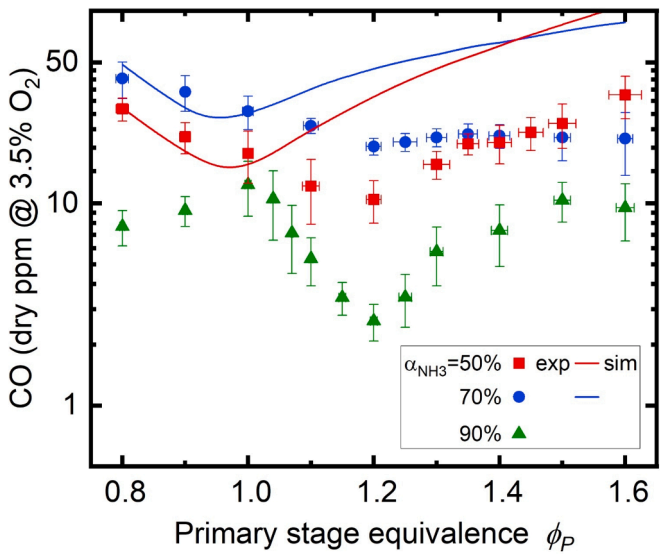

Fig. 8. CO emissions at different α_{NH_3} in the air-staged PM burner (Q_B = 0.5 MW/m^2).

In Fig. 5, there are a few points do not meet the predicted trend. These points refer mostly to the very fuel-lean or very fuel rich mixtures when pure NH_3 is burnt. Shown in Fig. 3, only strongly-burning NH_3-only flames ($1.0 < \phi_P < 1.4$) can be kept at the submerged flame mode at Q_B of 0.5 MW/m^2. For the attached flame mode, though the flames exist in the secondary stage and was attached to PM in primary stage, they burn insufficiently. The results indicate that for PM combustion of NH_3 blended fuels, keeping the flames in submerged flame mode is needed for low pollutant emissions.

Fig. 6 shows that the blending of auxiliary fuels (e.g., CH_4) promotes the conversion of fuel nitrogen to NOx in a wide range of ϕ_p. The vertical coordinate NOx conversion rate represents the proportion of nitrogen from NH_3 in the fuel that is converted to nitrogen in NOx. There is an optimal ϕ_p at which the NOx conversion is minimum. Both the optimal ϕ_p and the NOx conversion rate decrease with the increasing of NH_3 blending ratios (α_{NH_3}), rather than remaining at a constant. In another word, less NH_3 is converted into NOx per unit mass at a high α_{NH_3}. This is a benefit for porous media combustion, since porous media could increase the NH_3 combustion rate, stabilizing the flame at a low blending rate of auxiliary fuels or even at pure NH_3 combustion.

Fig. 7 depicts the measured NH_3 concentration in flue gas at different ϕ_P's for air-staging PM combustion. Consistent with observations, a little amount of unburnt NH_3 are produced due to the local blow-outs or quenching. However, this phenomenon is difficult to predict with the 1-D model. For the weakly-burning flames ($\phi_P < 1.0$ or $\phi_P > 1.4$), the lower flame speeds lead to more severe local quenching and a higher unburnt NH_3. For the pure NH_3 combustion illustrated by black dots, the weakly-burning flames have high unburnt NH_3 of about 1000 ppm and more.

Fig. 8 shows the variation of CO emissions with ϕ_P at three α'_{NH_3}s. In all cases, CO emissions are rather low. In general, on the fuel-rich side, CO emission becomes higher when more CH_4 exists in the fuel mixture, i.e., at a smaller α_{NH_3} . On the fuel-lean side, CO emission at α_{NH_3} = 50% is slightly lower than that at α_{NH_3} = 70%. This could be attributed to the more intensive combustion at a lower α_{NH_3}. At a low α_{NH_3}(50% −70%), the model well predicts the CO emission trends, and for a high α_{NH_3} (90%), the model shows no CO is emitted. Nevertheless, the results indicate that the CH_4-blended NH_3 combustion in air-staged PM burner does not lead to a high CO emission. The difference of CO emissions between the measurement and predictions could be mainly caused by the heat loss of the wall. In the modeling, though constant wall temperature was adopted, the PM radial temperature was assumed to be

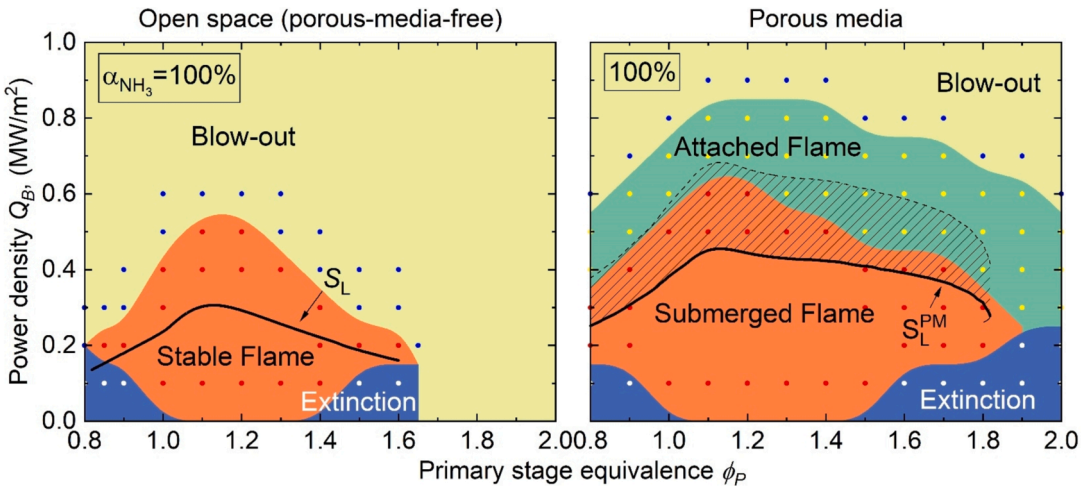

Fig. 9. Flame stability diagrams in PM and PM-free pure NH_3 combustion.

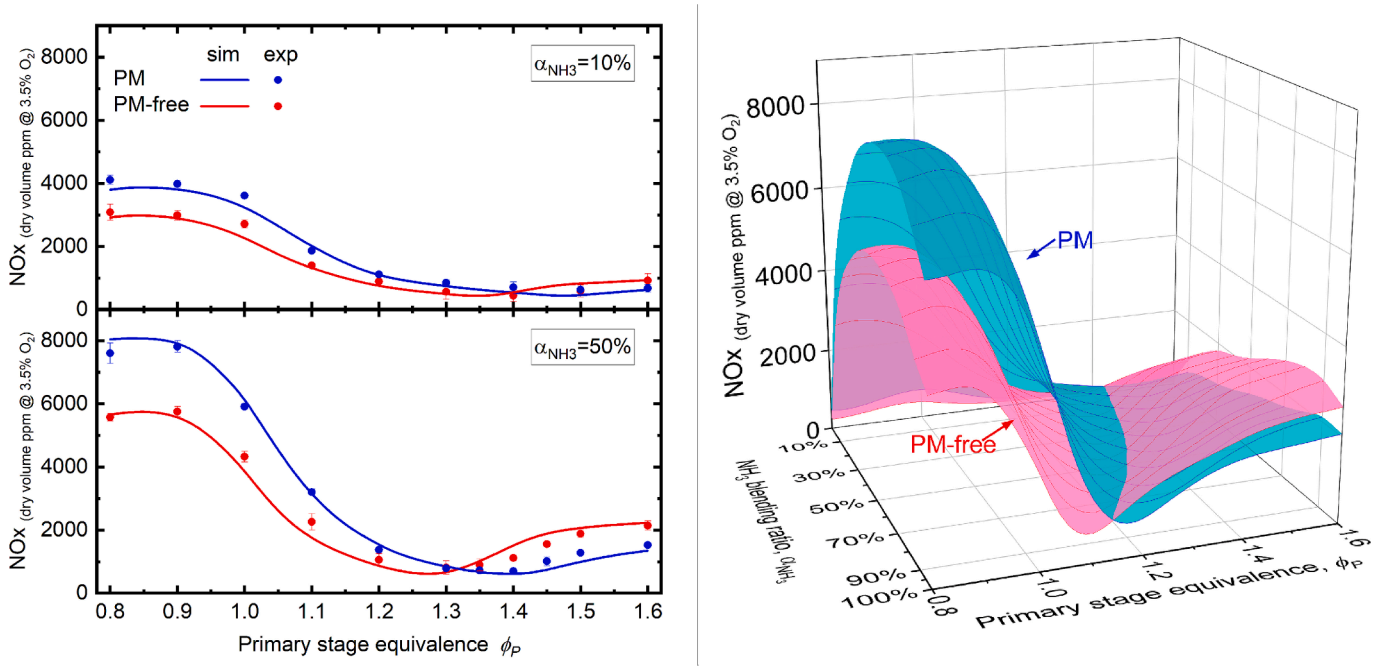

Fig. 10. The comparisons of NOx emission from NH_3/CH_4 air-staging combustion with and without PM at different α_{NH_3} (Q_B = 0.5 MW/m^2).

uniform (1-D approximation), which was in favor of CO depletion.

3.4. Porous media effect on flame stability

Fig. 9 shows the PM effect on the flame stability of pure NH_3 combustion, comparing the stability diagrams in PM and PM-free combustors. PM significantly increases the submerged flame mode zone, broadening the flammable region. In addition, it allows flames to be stabilized in the secondary stage as attached flame instead of being blown out. The area of blow-out region becomes much smaller.

Fig. 10 summarizes the PM effect on the NOx emission for CH_4-blended NH_3 combustion. Compared with results of PM-free flames, PM increases NOx emissions when the $\phi_P < \phi_{opt}$. When $\phi_P \geq \phi_{opt}$, PM is in favor of lower NOx emissions. It can be found that PM slightly decreases the minimum NOx emission at ϕ_{opt}. Adding PM has a similar effect on NOx emissions as reducing α_{NH_3} (adding auxiliary fuel CH_4). Heat feedback in PM preheats the unburnt reactants and increases the flame temperature and the reaction rate, like the addition of CH_4. It is worth to point out that though both PM and CH_4-blending enhance NH_3 combustion and increase the ϕ_{opt}, the associated mechanisms are different. The effect PM is attributed to the heat transfer enhancement, whereas the effect of CH_4-blending is attributed to the change of the nitrogen content and enhancement of chemical reactions.

In addition to enhancing combustion stability and altering NOx generation characteristics, the PM also contributes to the reduction of pollutant emissions in NH_3/CH_4 staged combustion. Fig. 11 illustrates the PM effect on various pollutants when α_{NH_3} = 70 %. The PM facilitates thermal transfer between the two combustion stages, allowing heat feedback from the secondary stage to the primary stage. Consequently, for pollutants like CO and NH_3, resulting from incomplete combustion, the PM can effectively reduce their emissions with rich-lean staged combustion. Furthermore, the PM also contribute to decreased NOx emissions with staged combustion. Experimental results at α_{NH_3} of 30–50 % (Fig. 10) and 70 % (Fig. 11) demonstrate that the addition of PM increase the ϕ_{opt} while slightly reducing NOx emissions at the ϕ_{opt}.

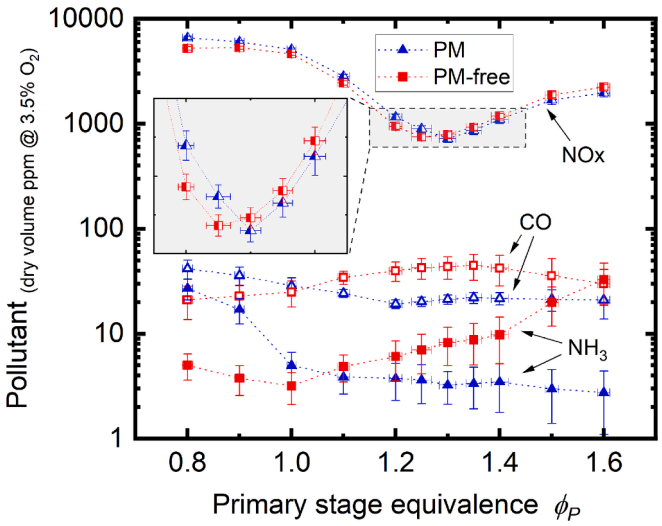

Fig. 11. Pollutant emissions in PM and PM-free air-staged burner (α_{NH_3} = 70 %, Q_B = 0.5 MW/m^2).

3.5. Influence of PPI

Fig. 12 shows the images of the CH_4/NH_3 flame in three SiC porous blocks with different PPIs. CT scanning shows that these three porous blocks have similar porosity and tortuosity, but with different mean pore diameters. Corresponding to 15, 10 and 5 PPI, their measured mean pore diameters are 2.40 mm, 3.21 mm and 3.92 mm respectively. As shown in Fig. 12, the porous blocks with larger pore have a stronger flame retention effect and a larger range of the submerged flame. Although with smaller volumetric heat transfer coefficients and weaker radiation heat transfer, larger pores allow for more significant conical protrusion of flame in the cavity. In the experiments, the staged combustion was not employed for the observation of the blow-out process in PM combustion, and the ϕ represents the premixed equivalence ratio for single-stage combustion.

3.6. Influence of air-staging distance

To further reduce NOx emission in air-staged PM burner, the process of NO generation at ϕ_{opt} was analyzed. In the primary stage, under the reducing atmosphere, NOx and NHx are reduced to N_2 by the reactions R(1) and R(2). When the atmosphere changes to oxidizing by the addition of the secondary air, the NHx is oxidized rapidly to form NOx. Since reducing reactions R(1) and R(2) are rather slow, increasing the residence time of the primary stage region may further reduce the NOx emissions at ϕ_{opt}.

$$NH + HNO \rightarrow N_2 + H_2O \quad (R1)$$

$$NH_2 + NO \rightarrow N_2 + H_2O \quad (R2)$$

The influence of air-staging distance x_s on NOx emissions under different ϕ_P's is shown in Fig. 13. The residence time also changes with ϕ_P, so it is more reasonable to compared the results at the same ϕ_P. For the conditions shown in Fig. 13, the primary stage residence time is estimated at 70 ms in stoichiometric conditions for a 15 mm thick PM. The experimental results show that increasing the primary stage residence time can further reduce NOx emissions with air-staging only around ϕ_{opt}, while the simulation results show it could also reduce NOx emissions in high ϕ_p conditions.

4. Conclusions

The present experimental and numerical study showed that the combination of air-staging and CH_4-blending to burn NH_3 in PM (porous media) burner is feasible and can overcome the difficulties of low flame speed, narrow flammability, high NOx and unburnt emissions encountered in direct NH_3 combustion. However, the PM effect on NOx

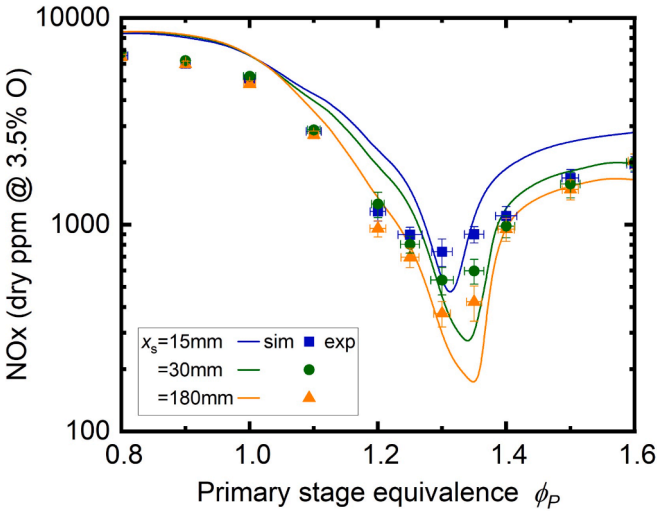

Fig. 13. NOx emissions for the air-staged PM burner with different air-staging distance (α_{NH_3} = 70 %, Q_B = 0.9 MW/m^2).

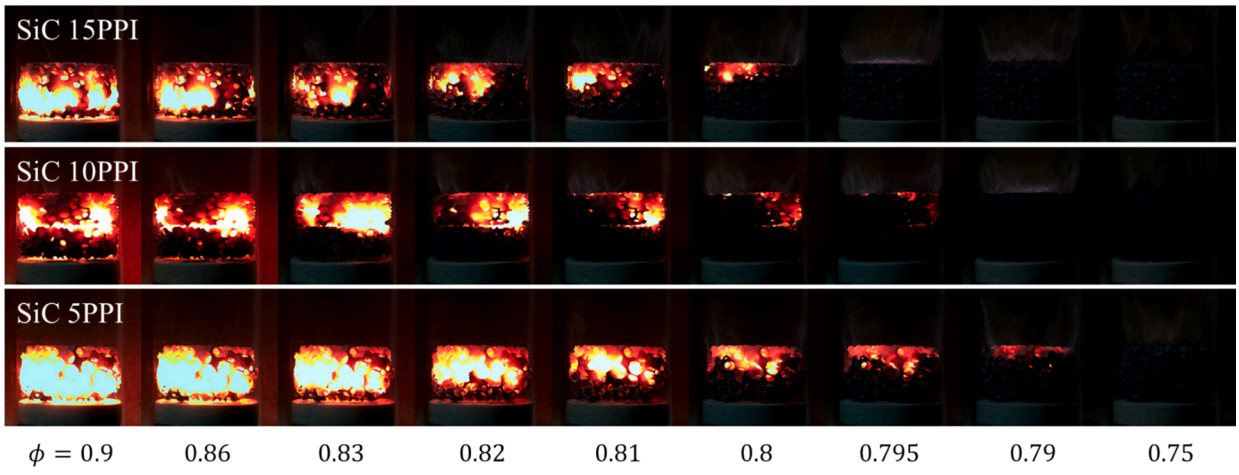

Fig. 12. Images of CH_4-blending NH_3 flames at different ϕ in PM with three apparent pore densities (α_{NH_3} = 70 %, Q_B = 0.9 MW/m^2).

emission depended on the local equivalence ratio of the mixtures. The proper selection of the equivalence ratio in the primary stage ϕ_P is important for the NOx emission control.

The variation of NOx emission with ϕ_P showed a V-shaped trend and there was an optimal ϕ_P (ϕ_{opt}) at which the NOx emission was minimum. Both PM and CH_4-blending increased ϕ_{opt}, while the associated mechanisms were different. The effect PM was attributed to the heat transfer enhancement, whereas the effect of CH_4-blending was attributed to the change of the nitrogen content and enhancement of chemical reactions. When $\phi_P < \phi_{opt}$, PM enhanced the NOx emission while when $\phi_P \geq \phi_{opt}$, it reduced the NOx emission.

The enhanced flame stability achieved with PM combustion contributed to the reduction of unburnt NH_3 and CO emissions. Notably, it was the submerged flame mode that played a significant role in minimizing these unburned emissions. PM slightly decreased the NOx emission at ϕ_{opt}, and significantly reduced unburnt NH_3 and CO emissions with air-staged combustion.

PM with large mean pore diameter was in favor of the presence of submerged flame and thus higher flame stability. Increasing the residence time in the primary stage was beneficent to reduce NOx emission around optimal ϕ_P. By optimizing the PM burner, the NOx emission of the burner was reduced to ~ 400 ppm (3.5 % O_2) at a high thermal power density of 0.9 MW/m^2 for 70 % NH_3 blended fuel.

CRediT authorship contribution statement

Liang Li: Writing – original draft, Methodology, Investigation. **Ruifang Zhang:** Investigation. **Yang Zhang:** Validation, Project administration, Funding acquisition. **Hai Zhang:** Writing – review & editing, Validation, Project administration, Conceptualization.

Declaration of competing interest

The authors declare that they have no known competing financial interests or personal relationships that could have appeared to influence the work reported in this paper.

Acknowledgement

This work is supported by the National Natural Science Foundation of China (Grant # 52176116) and the Key Technology Projects of Taiyuan (2024TYJB0101). The author Y. Zhang receives the support from the Seed Fund of Shanxi Research Institute For Clean Energy Tsinghua University.

Data availability

Data will be made available on request.

References

[1] Elbaz AM, Wang S, Guiberti TF, Roberts WL. Review on the recent advances on ammonia combustion from the fundamentals to the applications. Fuel Commun 2022;10:100053. https://doi.org/10.1016/j.jfueco.2022.100053.
[2] Roy D, Roy S, Smallbone A, Roskilly AP. Assessing the techno-economic viability of a trigeneration system integrating ammonia-fuelled solid oxide fuel cell. Appl Energy 2024;357:122463. https://doi.org/10.1016/j.apenergy.2023.122463.
[3] Lhuillier C, Brequigny P, Contino F, Mounaïm-Rousselle C. Experimental study on ammonia/hydrogen/air combustion in spark ignition engine conditions. Fuel 2020; 269:117448. https://doi.org/10.1016/j.fuel.2020.117448.
[4] Ryu K, Zacharakis-Jutz GE, Kong S-C. Performance characteristics of compression-ignition engine using high concentration of ammonia mixed with dimethyl ether. Appl Energy 2014;113:488–99. https://doi.org/10.1016/j.apenergy.2013.07.065.
[5] Tamura M, Gotou T, Ishii H, Riechelmann D. Experimental investigation of ammonia combustion in a bench scale 1.2 MW-thermal pulverised coal firing furnace. Appl Energy 2020;277:115580. https://doi.org/10.1016/j.apenergy.2020.115580.
[6] Valera-Medina A, Pugh DG, Marsh P, et al. Preliminary study on lean premixed combustion of ammonia-hydrogen for swirling gas turbine combustors. Int J Hydrog Energy 2017;42:24495–503. https://doi.org/10.1016/j.ijhydene.2017.08.028.
[7] Kurata O, Iki N, Matsunuma T, et al. Performances and emission characteristics of NH_3–air and NH_3CH_4–air combustion gas-turbine power generations. Proc Combust Inst 2017;36:3351–9. https://doi.org/10.1016/j.proci.2016.07.088.
[8] Kobayashi H, Hayakawa A, Somarathne KDKA, Okafor EC. Science and technology of ammonia combustion. Proc Combust Inst 2019;37:109–33. https://doi.org/10.1016/j.proci.2018.09.029.
[9] Valera-Medina A, Marsh R, Runyon J, et al. Ammonia–methane combustion in tangential swirl burners for gas turbine power generation. Appl Energy 2017;185: 1362–71. https://doi.org/10.1016/j.apenergy.2016.02.073.
[10] Afif A, Radenahmad N, Cheok Q, et al. Ammonia-fed fuel cells: a comprehensive review. Renew Sustain Energy Rev 2016;60:822–35. https://doi.org/10.1016/j.rser.2016.01.120.
[11] Hayakawa A, Goto T, Mimoto R, et al. Laminar burning velocity and Markstein length of ammonia/air premixed flames at various pressures. Fuel 2015;159: 98–106. https://doi.org/10.1016/j.fuel.2015.06.070.
[12] Han X, Wang Z, Costa M, et al. Experimental and kinetic modeling study of laminar burning velocities of NH_3/air, NH_3/H_2/air, NH_3/CO/air and NH_3/CH_4/air premixed flames. Combust Flame 2019;206:214–26. https://doi.org/10.1016/j.combustflame.2019.05.003.
[13] Um DH, Joo JM, Lee S, Kwon OC. Combustion stability limits and NOx emissions of nonpremixed ammonia-substituted hydrogen–air flames. Int J Hydrog Energy 2013;38:14854–65. https://doi.org/10.1016/j.ijhydene.2013.08.140.
[14] Ichikawa A, Hayakawa A, Kitagawa Y, et al. Laminar burning velocity and Markstein length of ammonia/hydrogen/air premixed flames at elevated pressures. Int J Hydrog Energy 2015;40:9570–8. https://doi.org/10.1016/j.ijhydene.2015.04.024.
[15] Miller JA, Bowman CT. Mechanism and modeling of nitrogen chemistry in combustion. Prog Energy Combust Sci 1989;15:287–338. https://doi.org/10.1016/0360-1285(89)90017-8.
[16] Hayakawa A, Goto T, Mimoto R, et al. NO formation/reduction mechanisms of ammonia/air premixed flames at various equivalence ratios and pressures. Mech Eng J 2015;2:14–00402. https://doi.org/10.1299/mej.14-00402.
[17] Li T, Duan Y, Wang Y, Zhou M, Duan L. Research progress of ammonia combustion toward low carbon energy. Fuel Process Technol 2023;248:107821. https://doi.org/10.1016/j.fuproc.2023.107821.
[18] Huo Y, Zhang R, Zhu S, Gao J, Holden SR, Zhu M, et al. A Preliminary Experimental Investigation into Ammonia Oxidization in a Fixed Bed. Int J Energy Clean Environ 2022;23:23–37. https://doi.org/10.1615/InterJEnerCleanEnv.2022039811.
[19] Ju Y, Maruta K. Microscale combustion: Technology development and fundamental research. Prog Energy Combust Sci 2011;37:669–715. https://doi.org/10.1016/j.pecs.2011.03.001.
[20] Hsu P-F, Howell JR, Matthews RD. A numerical investigation of premixed combustion within porous inert media. J Heat Transf 1993;115:744–50. https://doi.org/10.1115/1.2910746.
[21] Francisco RW, Costa M, Catapan RC, Oliveira AAM. Combustion of hydrogen rich gaseous fuels with low calorific value in a porous burner placed in a confined heated environment. Exp Therm Fluid Sci 2013;45:102–9. https://doi.org/10.1016/j.expthermflusci.2012.10.011.
[22] Huang R, Cheng L, Qiu K, Zheng C, Luo Z. Low-calorific gas combustion in a two-layer porous burner. Energy Fuels 2016;30(2):1364–74. https://doi.org/10.1021/acs.energyfuels.5b02399.
[23] Gharehghani A, Ghasemi K, Siavashi M, Mehranfar S. Applications of porous materials in combustion systems: A comprehensive and state-of-the-art review. Fuel 2021;304:121411. https://doi.org/10.1016/j.fuel.2021.121411.
[24] Habib R, Yadollahi B, Saeed A, et al. Unsteady ultra-lean combustion of methane and biogas in a porous burner – An experimental study. Appl Therm Eng 2021;182: 116099. https://doi.org/10.1016/j.applthermaleng.2020.116099.
[25] Sharma D, Lee BJ, Dash SK, Reddy VM. Experimental and numerical investigation on ultra-high intensity premixed LPG- air combustion in a novel porous stack burner. Energy 2023;272:127148. https://doi.org/10.1016/j.energy.2023.127148.
[26] Nozari H, Karaca G, Tuncer O, Karabeyoglu A. Porous medium based burner for efficient and clean combustion of ammonia–hydrogen–air systems. Int J Hydrog Energy 2017;42:14775–85. https://doi.org/10.1016/j.ijhydene.2017.03.234.
[27] Chen D, Li J, Li X, Deng L, et al. Study on combustion characteristics of hydrogen addition on ammonia flame at a porous burner. Energy 2023;263:125613. https://doi.org/10.1016/j.energy.2022.125613.
[28] Vignat G, Akoush B, Toro ER, Boigné E, Ihme M. Combustion of lean ammonia-hydrogen fuel blends in a porous media burner. Proc Combust Inst 2023;39: 4195–204. https://doi.org/10.1016/j.proci.2022.07.054.
[29] Vignat G, Zirwes T, Toro ER, Younes K, Boigné E, Muhunthan P, et al. Experimental and numerical investigation of flame stabilization and pollutant formation in matrix stabilized ammonia-hydrogen combustion. Combust Flame 2023;250: 112642. https://doi.org/10.1016/j.combustflame.2023.112642.
[30] Somarathne KDKA, Hatakeyama S, Hayakawa A, Kobayashi H. Numerical study of a low emission gas turbine like combustor for turbulent ammonia/air premixed swirl flames with a secondary air injection at high pressure. Int J Hydrog Energy 2017;42:27388–99. https://doi.org/10.1016/j.ijhydene.2017.09.089.
[31] Rocha RC, Costa M, Bai X-S. Combustion and Emission Characteristics of Ammonia under Conditions Relevant to Modern Gas Turbines. Combust Sci Technol 2021; 193:2514–33. https://doi.org/10.1080/00102202.2020.1748018.
[32] Yamashita H, Hayakawa A, Okafor EC, et al. Optimum primary equivalence ratio for rich-lean two-stage combustion of non-premixed ammonia/methane/air and

ammonia/hydrogen/air flames in a swirling flow. Fuel 2024;368:131598. https://doi.org/10.1016/j.fuel.2024.131598.
[33] Li Z, Zhang Y, Zhang H. Kinetics modeling of NOx emission of oxygen-enriched and rich-lean-staged ammonia combustion under gas turbine conditions. Fuel 2024; 355:129509. https://doi.org/10.1016/j.fuel.2023.129509.
[34] Wang X, Fan W, Chen J, Feng G, Zhang X. Experimental study on effects of air-staged strategy and NH_3 co-firing ratios on NO formation characteristics in ammonia/coal co-firing process. Fuel 2023;332:126217. https://doi.org/10.1016/j.fuel.2022.126217.
[35] Cooper SJ, Bertei A, Shearing PR, et al. An open-source application for calculating tortuosity factors from tomographic data. SoftwareX 2016;5:203–10. https://doi.org/10.1016/j.softx.2016.09.002.
[36] Rabbani A, Jamshidi S, Salehi S. An automated simple algorithm for realistic pore network extraction from micro-tomography images. J Pet Sci Eng 2014;123: 164–71. https://doi.org/10.1016/j.petrol.2014.08.020.
[37] Howell JR, Hall MJ, Ellzey JL. Combustion of hydrocarbon fuels within porous inert media. Prog Energy Combust Sci 1996;22:121–45. https://doi.org/10.1016/0360-1285(96)00001-9.
[38] Wu Z, Caliot C, Flamant G, Wang Z. Numerical simulation of convective heat transfer between air flow and ceramic foams to optimise volumetric solar air receiver performances. Int J Heat Mass Transf 2011;54:1527–37. https://doi.org/10.1016/j.ijheatmasstransfer.2010.11.037.
[39] Baillis D, Raynaud M, Sacadura JF. Determination of spectral radiative properties of open cell foam: model validation. J Thermophys Heat Transf 2000;14:137–43. https://doi.org/10.2514/2.6519.
[40] Okafor EC, Naito Y, Colson S, Ichikawa A, Kudo T, Hayakawa A, et al. Experimental and numerical study of the laminar burning velocity of CH4–NH3–air premixed flames. Combust Flame 2018;187:185–98. https://doi.org/10.1016/j.combustflame.2017.09.002.
[41] Konnov AA. Implementation of the NCN pathway of prompt-NO formation in the detailed reaction mechanism. Combust Flame 2009;156:2093–105. https://doi.org/10.1016/j.combustflame.2009.03.016.
[42] Li R, Konnov AA, He G, Qin F, Zhang D. Chemical mechanism development and reduction for combustion of NH3/H2/CH4 mixtures. Fuel 2019;257:116059. https://doi.org/10.1016/j.fuel.2019.116059.
[43] Zhang H, Fan R, Wang S, et al. Extinction of lean near-limit methane/air flames at elevated pressures under normal- and reduced-gravity. Proc Combust Inst 2011;33: 1171–8. https://doi.org/10.1016/j.proci.2010.06.027.
[44] Zheng C, Cheng L, Saveliev A, Luo Z, Cen K. Numerical studies on flame inclination in porous media combustors. Int J Heat Mass Transf 2011;54:3642–9. https://doi.org/10.1016/j.ijheatmasstransfer.2011.02.066.